Biomedical Engineering: Applications, Basis and Communications, Vol. 28, No. 6 (2016) 1650042 (12 pages)
DOI: 10.4015/S1016237216500423

World Scientific
www.worldscientific.com

# TOWARD A COMPUTER AIDED DIAGNOSIS SYSTEM FOR LUMBAR DISC HERNIATION DISEASE BASED ON MR IMAGES ANALYSIS

Mehran Nikravan*, Elias Ebrahimzadeh†,§, Mohammad Rasool Izadi‡ and Mohammad Mikaeili*

*Department of Biomedical Engineering
Shahed University, Tehran, Iran

†School of Electrical and Computer Engineering
College of Engineering, University of Tehran, Tehran, Iran

‡Department of Electrical Engineering
Sharif University of Technology, Tehran, Iran

Accepted 26 October 2016
Published 19 December 2016

## ABSTRACT

Lumbar disc diseases are the commonest complaint of Lower Back Pain (LBP). In this paper, a new method for automatic diagnosis of lumbar disc herniation is proposed which is based on clinical Magnetic Resonance Images (MRI) data. We use T2-W sagittal and myelograph images. Our method uses Otsu thresholding method to extract the spinal cord from MR images of Lumbar disc. In the next step, a third-order polynomial is aligned on the extracted spinal cords, and in the end of preprocessing step all the T2-W sagittal images are prepared for extracting disc boundary and labeling. After labeling and extracting a ROI for each disc, intensity and shape features are used for classification. The presented Method is applied on 30 clinical cases, each containing 7 discs (210 lumbar discs) for the herniation diagnosis. The results revealed 92.38% and 93.80% accuracy for Artificial Neural Network and Support Vector Machine (SVM) classifiers, respectively. The results indicate the superiority of the proposed method to those mentioned in similar studies.

*Keywords*: Lumbar disc diseases; LBP; Automatic diagnosis; Herniation; MRI; Myelograph; Spinal cord.

## INTRODUCTION

Lumbar disc diseases are the most wide-spread complaints for Lower Back Pain (LBP).[1] Herniation in the lumbar area is one of the most common diseases that results in LBP.[2] Herniation is a disease in which disc substance compress the spinal cord and roots. The degree of lesions depends on nucleus pulposus state. The first stage is called bulging, in which the annulus fibrosis is intact and the disc has a mild herniation with a little compression on ligaments and spinal cord. In the second stage (called protrusion), the herniated disc breaks the inner ligaments and compresses the spinal cord or roots. In the third stage, called extrusion, the disc substance breaks all ligaments except outer ones, and the compression on spinal cord and roots is considerable. In this situation, herniated disc has a free fragment. In another kind of herniation, the free fragment part migrates superiorly. In the fourth stage, there is herniated disc with

§Corresponding author. Elias Ebrahimzadeh, Ph.D. Student of Biomedical Engineering, School of Electrical and Computer Engineering, College of Engineering, University of Tehran, Tehran, Iran. E-mail: e_ebrahimzadeh@ut.ac.ir, elias.ebrahimzadeh@yahoo.com

a free fragment that has ruptured through the posterior ligaments and is against the thecal sac.[3] A Computer Aided Diagnosis (CAD) system can be helpful to generate diagnostic results within a short time. In addition, it can be useful to increase precision of diagnosis and eliminate the effects of human errors caused by tiredness and inevitable visual errors of radiologists. Therefore, the need of tiresome analysis of the images by the physicians is unnecessary.[4] The spinal cords have wide variability including turning angle, size, shape, etc. Moreover abnormal pertaining conditions such as vertebral fusions, disc diseases and spinal infections add to these varieties.[5] The labeling and detection of lumbar disc is a necessary step to design a CAD system for automatic diagnosis of lumbar area diseases like herniation on clinical MR images. Some radiologists make use of CT to detect Back disorders. Clinically speaking, MRI provides images with higher resolution. Furthermore, due to the higher safety of MRI in comparison to the radiative emission of CT, MRI is a more suitable method for this purpose. CT is usually used in the situations where the disease is located inside bone structures such as injuries to back bones. By the way, this issue is not within the scope of this study. Figure 1 depicts the MR image which is extracted from the dataset.

In this study, we present a new method for disc labeling by means of fitting a third-order polynomial on extracted spinal cord region from Magnetic Resonance Imaging (MRI) and Magnetic Resonance Myelographic (MRM) images. After labeling and Region of Interest (ROI) selection in the discs limited area, our method generates the features, and diagnoses lumbar disc herniation by means of Artificial Neural Network and Support Vector Machine (SVM). Classifiers automatic lumbar disc diseases diagnosing has been developed in many of the previous works. These studies investigated a


**Fig. 1** T2-weighted MR sagittal view of lumbar region.

computer-based method for the diagnosis of disc degeneration.[6–8] Michopoulou *et al.*[9] developed a fuzzy-c means classifier to perform normal and degenerated segmentation. This method was semi-automatic and achieved 86–88% accuracy on 34 cases. Tsai *et al.* used geometrical features (shape, size and location) to diagnose herniation from 3D MRI and CT axial (transverse sections) volumes of the discs.[10] Jarvik and Deyo compared the performance of several algorithms in terms of specificity and sensitivity. In addition, they showed relative frequency of low back pain according to symptoms of back pain only, sciatica, or possible stenosis.[11] They also suggested an algorithm for the diagnostic evaluation of patients with low back pain using history, physical exams and imaging studies. Graaf *et al.* compared 15 imaging tests and 7 clinical tests in terms of the diagnostic accuracy in detecting lumbar spinal stenosis. They claimed that clinical tests showed substantial variation and there was no confirmation about the superiority of the diagnostic performance among the different tests.[12] Bounds *et al.*[13] utilized a neural network for diagnosis of back pain and sciatica. Sciatica might be caused by lumbar disc herniation as well as many other reasons. They had three groups of doctors to perform diagnosis as their validation mechanism. They achieved better accuracy than the doctors in the diagnosis. Wildermuth *et al.* quantitatively assessed MRI and MRM in terms of the sagittal diameter of the lumbar dural sac.[14] Forty subjects were participated in this study and they claimed that MRI and MRM are comparable since the correlation between them is high (i.e., $r = 0.81–0.97$). They argued that there are a strong correlation between MRI and MRM but did not mention the applicability of these two modalities to CAD. Vaughn conducted a research study on using neural network for assisting orthopedic surgeons in the diagnosis of lower back pain. This research team classified LBP into three broad clinical categories.[15] They used 25 features to train the Neural Network (NN) including symptoms clinical assessment results. The NN achieved 99% of training accuracy and 78.5% of testing accuracy. These results show, the overfitting in training data. Roberts *et al.*[16] employed watershed techniques for automatic detection of intervertebral discs from a combination of proton density (PD) and T2-weighted MR images. Also, in other work Roberts *et al.*[17] used ASM to detect and quantify vertebral fracture from X-ray radiographs for the lumbar and thoracic area (L4 up to T7) using extracted shape and appearance features for performing quantitative fracture classification. Because of differences in vertebrae, they trained a shape model for each of three classes: upper thoracic (T7-T9), lower thoracic (T10-T12), and lumbar (L1-L4). They presented a

comparison study between appearance and shape effect on classification in each vertebral group. Chevrefils *et al.*[18] utilized a combination of watershed and morphological operations to detect the discs from MR images. Recently, Alumari *et al.* used Gradient Vector Flow (GVF)-snake and designed a Gibbs-based classifier to classify each disc as either normal or herniated.[19] In the sections, we discuss Methods and Materials consists of Dataset, previous related works, feature extraction, Our Method (Sec. 2), Experimental results of our method (Sec. 3), Discussion (Sec. 4) and finally Conclusion (Sec. 5) in detail, respectively.

## METHODS AND MATERIALS

### Dataset

The used data were obtained with a 1.5-T MR imaging system (Siemens) from subjects aged between 21 and 73 years. Each case comprises 7 slices. In this study, we used just T2-W sagittal (30 images) and MRM series (30 images) for diagnosis. In the set of T2-W sagittal images (9 images) the best one is the fifth image. The parameters of imaging was: flip angle of 150° for both T2-W sagittal and MRM, echo time of 121 ms, repetition time of 3100 ms, field of view (FOV) 32 cm for T2-W sagittal, echo time of 1300 ms, repetition time of 10,000 ms, and FOV 35 cm for MRM images. The images, labeled by the radiologists, contain 12 normal subjects and 18 patients. Each person has 2.66 disc herniation on average (8 persons with 3 disc herniation, 6 with 2 disc herniation, and 4 with one disc herniation.)

### Proposed Approach for Intervertebral Disc Labeling

In this paper, the proposed approach is a new method for boundary detection to be used in CAD for diagnosis of lumbar disc herniation based on magnetic resonance images (MRI). We discriminate and label the intervertebral discs automatically using a combination of different algorithms including Otsu thresholding, Morphological operations in order to improve the images and a third-order polynomial function to fit on spinal canal.

### Otsu Thresholding Method

We applied Otsu automatic thresholding approach to extract spinal canal,[20–22] It is essential to select an appropriate threshold of gray level to extract a specific object through image processing. A lot of techniques for object discrimination have been developed and used until now. Suppose that the established image has $N$ pixels and the gray level of pixels are between 1 and $L$. If the number of pixels with gray level $i$ is depicted by $n_i$, probability distribution function for each gray level $i$ will be equal to:

$$p_i = \frac{n_i}{N}, \quad p_i \geq 0, \sum_{i=1}^{L} p_i = 1. \tag{1}$$

Let us suppose that pixels of the image fall into two subgroups called $C_0$ and $C_1$ with the threshold of $K$ for gray level. The gray level of pixels in $C_0$ and $C_1$ subgroups is within the intervals of [1, 2,..., $K$] and [$K$+1,..., $L$], respectively. Now, it is possible to identify a probability distribution function and a mean for each subgroup. $\omega_0$ and $\omega_1$ are the probability distribution functions of $C_0$ and $C_1$ subgroups, respectively.

$$\omega_0 = P_r(C_0) = \sum_{i=1}^{K} P_i \tag{2}$$

$$\omega_1 = P_r(C_1) = \sum_{i=K+1}^{L} P_i = 1 - \omega_0 \tag{3}$$

and

$$\mu_0 = \sum_{i=1}^{K} iP_r(i|C_0) = \sum_{i=1}^{K} iP_i/\omega_0 = \frac{\mu(K)}{\omega(K)}, \tag{4}$$

$$\mu_1 = \sum_{i=K+1}^{L} iP_r(i|C_1) = \sum_{i=K+1}^{L} iP_i/\omega_1 = \frac{\mu_T - \mu(K)}{1 - \omega(K)}, \tag{5}$$

where

$$\omega(K) = \omega_0 = \sum_{i=1}^{K} P_i, \tag{6}$$

$$\mu(K) = \sum_{i=1}^{K} iP_i, \tag{7}$$

and

$$\mu_T = \mu(L) = \sum_{i=1}^{L} iP_i \tag{8}$$

$\mu_T$ is the average of the image and the following equations hold.

$$\omega_0\mu_0 + \omega_1\mu_1 = \mu_T, \quad \omega_0 + \omega_1 = 1. \tag{9}$$

The variances of $C_0$ and $C_1$ will be given by the following relations, respectively.

$$\delta_0^2 = \sum_{i=1}^{K} (i-\mu_0)^2 P_r(i\,|C_0) = \sum_{i=1}^{K} (i-\mu_0)^2 P_i/\omega_0, \quad (10)$$

$$\delta_1^2 = \sum_{i=K+1}^{L} (i-\mu_1)^2 P_r(i\,|C_1) = \sum_{i=K+1}^{L} (i-\mu_1)^2 P_i/\omega_1. \quad (11)$$

Using the below equation, Otsu method calculates the variances between the two subgroups in order to find a proper threshold:

$$\delta_B^2 = \omega_0(\mu_0 - \mu_T)^2 + \omega_1(\mu_1 - \mu_T)^2. \quad (12)$$

The optimized threshold depicted by $t^*$ will be calculated for $1 \leq t < L$

$$t^* = \arg\operatorname{Max}\{\delta_B^2(t)\}. \quad (13)$$

Equation (12) can be generalized to multilevel thresholding, If there are $M-1$ thresholds, shown by $\{t1, t2, \ldots, t_{M-1}\}$, the main image will fall into $M$ subgroups. So that subgroups $C_0$, $C_1$, and $C_{M-1}$ will have the following thresholds intervals $\{1, \ldots, t1\}, \{t1+1, \ldots, t2\}$, and $\{t_{M-1}+1, \ldots, L\}$, respectively and the optimized thresholds $\{t_1^*, t_2^*, \ldots, t_{M-1}^*\}$ will be selected by maximizing $\delta_B^2$

$$\delta_B^2 = \sum_{K=0}^{M-1} \omega_K(\mu_K - \mu_T)^2, \quad (14)$$

$$\omega_K = \sum_{i \in C_K} P_K, \quad (15)$$

And

$$\mu_K = \sum_{i \in C_K} i(P_i/\omega(K)) \quad (16)$$

$$\{t_1^*, t_2^*, \ldots, t_{M-1}^*\} = \arg\operatorname{Max}\{\delta_B^2(t_1 t_2, \ldots, t_{M-1})\}. \quad (17)$$

We follow the below instruction in order to extract spinal cord and detect a proper boundary for intervertebral discs:

Sagittal images of T2-weighted MRI are longitudinal slices. After studying all slices belonging to 30 patients it was determined that the spinal canal was depicted with higher resolution in slice number 5 (Fig. 2).

After investigating the image number 5 by means of trial and error, it is identified that only middle parts of the image are included in our ROI because the discs and spinal canal are located in this area of the image. Therefore, we remove right and left redundant parts to speed up the process and simplify the analyses. Figure 3 shows the main image after the removal of the useless areas.

As discussed in Sec. 3.2.1, we use automatic Otsu thresholding in order to extract spinal canal. In this method, discrimination and extraction of spinal canal is done by finding a distinct threshold automatically and dividing the gray level of pixels in a specific image into two classes. Figure 4 shows the images after applying the Otsu method. It is essential to refine the image of extracted spinal canal and prepare it for later processing. We did this primary processing by means of morphological operations and filtering methods. Figure 5 demonstrates results of such pre-processing operations. Besides T2 weighted sagittal MRI, another type of images called MRM is available for physicians to diagnose disc herniation. Spinal cord is identifiable in MRM images. Figure 6 demonstrates a sample of MRM images.

**Fig. 2** The 5th cut is the most proper one among nine slices.

**Fig. 3** Left: the original image. Right: image after removal and ROI selection.

**Fig. 4** Left: the original image after ROI selection. Right: image after extracting spinal canal based on one specific threshold.

Regarding the fact that the spinal cord images obtained from the preprocessed T2-weighted sagittal have lower quality than MRM images, in order to be able to align a more suitable third-order polynomial on it, we try to achieve better image in this process through matching these two images on each other, in a way that the spinal cord in these images would fit well on each other. Figure 7 shows the results of this matching used for fitting a third-order polynomial. To extract the

**Fig. 5** Picture of spinal canal after pre-processing operations and improvement.

**Fig. 6** MRM image.

boundary of discs, we first rotate Fig. 7, 90° and then fit a third-order polynomial on the spinal cord. Figure 8 shows the results of this alignment.

In the first stage, we tried to obtain a suitable binary image to reveal the discs. For this purpose, we converted

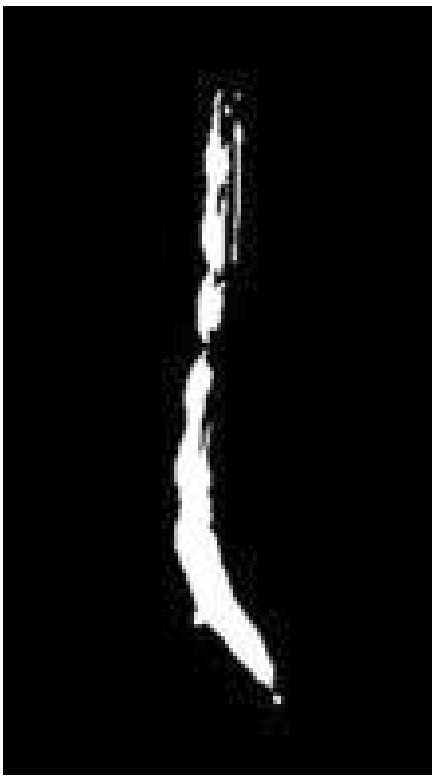

**Fig. 7** Result of matching Fig. 5 with MRM binary image.

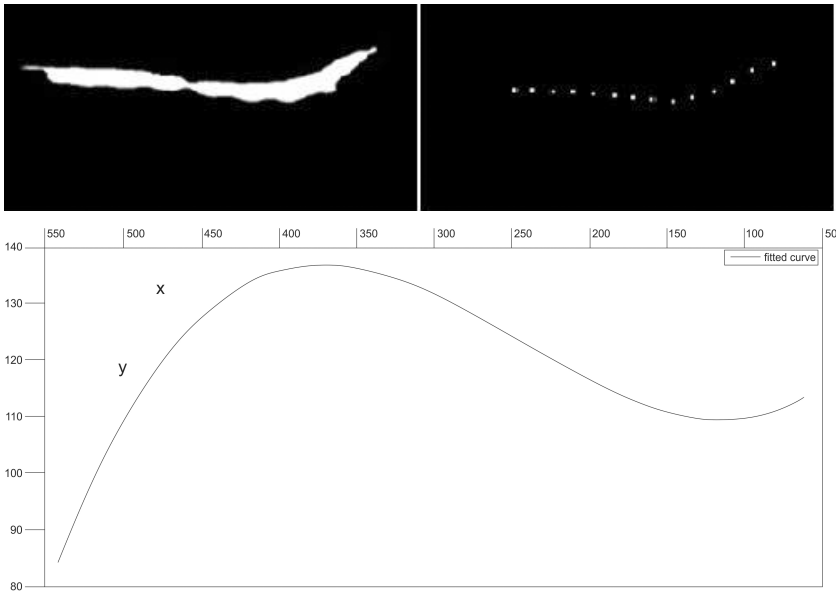


**Fig. 8** Top left: spinal cord after 90° rotation Top right: Tracking point on spinal cord Below: fitting third-order polynomial.

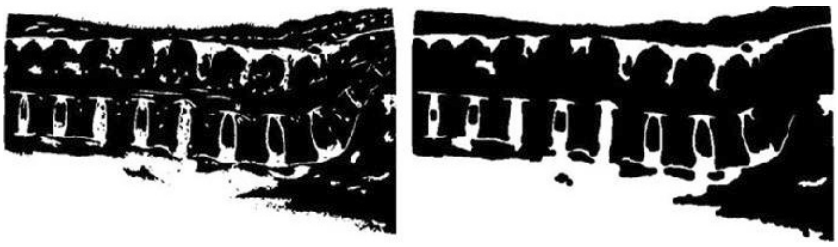

**Fig. 9** Left: binary image after applying threshold right: smooth image by means of morphological operators.

the image to black and white using a threshold in order to achieve a suitable binary image. Then by using morphological operations, we made this image smoother. Figure 9 depicts the resulting binary image and the image after conducting morphological operations. In order to extract the location of the discs, a 50*40-pixel rectangle has been slid longitudinally along the third order polynomial perpendicular to the curve (Fig. 10). The sliding steps were chosen empirically as 1/120 of the total curve length. The procedure of the discs' location extraction is as follows:

The aforementioned rectangle has been used as a mask on the binary image developed in the previous step (Fig. 9). At each 120 positions of the rectangle, we

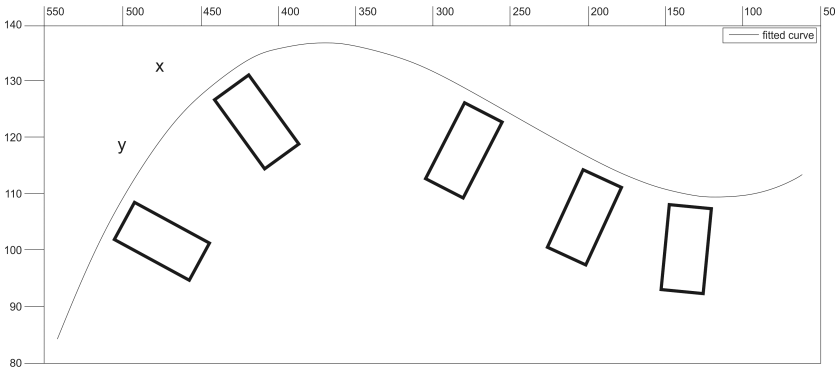


**Fig. 10** Sliding rectangle on third-order polynomial.

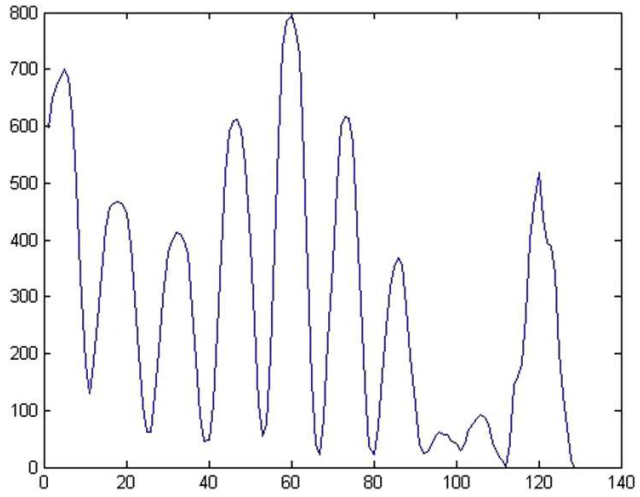


**Fig. 11** The peaks show the maximum overlap of the rectangle with discs in 120 step.

calculated the total number of the white pixels inside the masked area. This number is plotted against the step number in Fig. 11.

As illustrated in the above diagram, it can be concluded that, where the maximum overlapping between the rectangular area and the binary image's white pixels occurs, the location of one disc is found.

As mentioned earlier, each peak in the above diagram depicts a disc's place. It should be mentioned that the maximum points in Fig. 11 have been extracted by Pan–Tompkins algorithm.[23–26,a] In the second step of the process, by approaching each disc's location, another rectangular area with the size of 140∗70 pixels is placed on the image in a way that it covers the whole disc. The size of this rectangle has been determined through trial and error. These observations have been shown in Fig. 12. For disc labeling, we considered the diagram of illumination intensity. Figure 13 shows the intensity of the image's pixels through the length of the image. At each point, the intensity is calculated as the summation of the intensity of the pixels in each column of the image. With regards to this fact that the spinal cord area in disc image has higher resolution, the maximum X occurs at the spinal cord area. This characteristic is shown at the right side of the diagram. At first we calculate this maximum value ($X_1$) and then begin to find a peak at the left side of the diagram ($X_2$) which is at the left side of disc and is certainly out of the disc range. After achieving these two values for X, $X_1$ and $X_2$, we begin to obtain the mid value called $X_m$.

Then, at the dissection $X_m$, in direction to axis Y has been shown in Fig. 14, with using darkness of the lower and upper bound having the least intensity, we obtained the points related to the edge, named A and B in Fig. 14. In fact, with drawing this diagram in direction to dissection related to $X_m$, these two points as a minimum are specified, as shown in diagram of Fig. 14. So as mentioned, the lower and upper edges of disc were cut by vertical cutting $X_m$ in points A and B, and with respect to the modification of resolution of pixels at the direction to mid cutting, when cross from vertebra and enter to disc (point A) and as well when exit the disc (point B) in resolution diagram, we had two minimum which were Detectable easily and in such a way the points A and B were obtained. Then, for tagging process in appropriate point with in disc, the mid transverse point between A and B (point C in Fig. 15) was obtained and thus we could tag the specified discs with using this method.

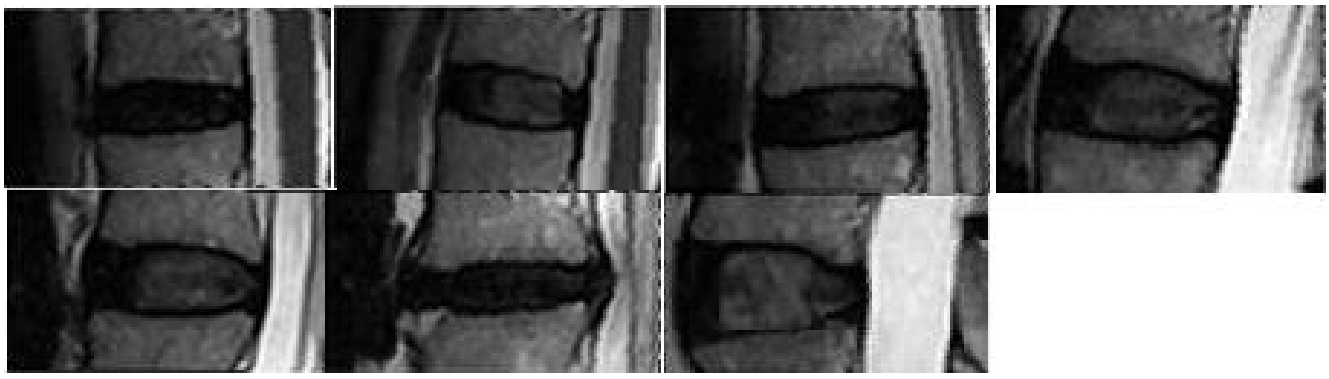

**Fig. 12** The extracted 7 lumbar discs.

[a]Reference 25: Article in Persian with an abstract in English.

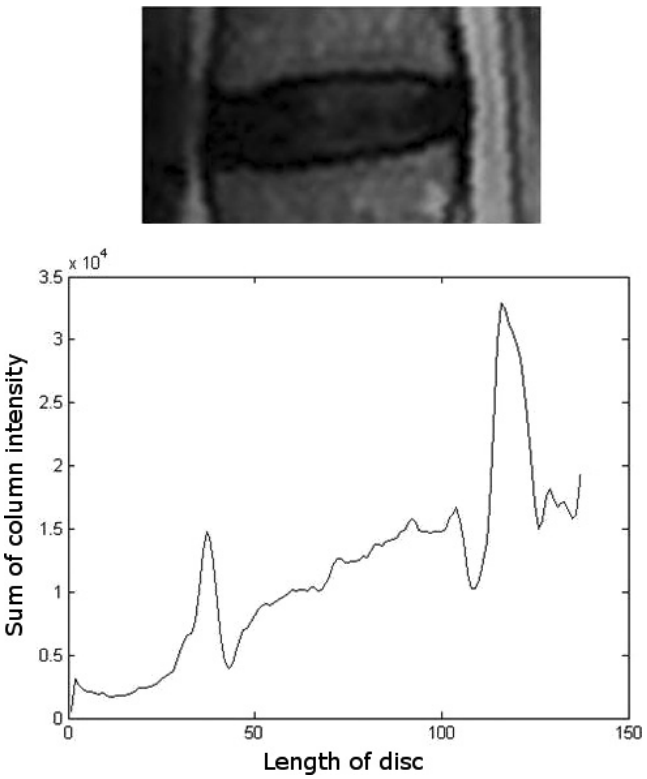


**Fig. 13** Disc and its intensity diagram.

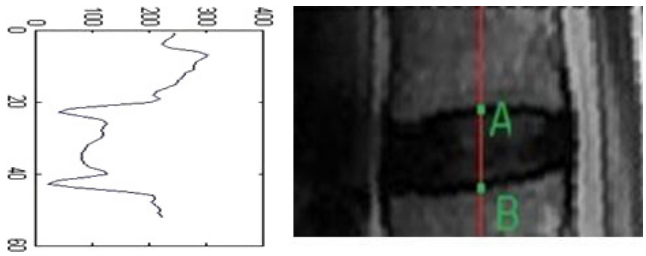


**Fig. 14** Disc image and its Intensity diagram in direction of red line.

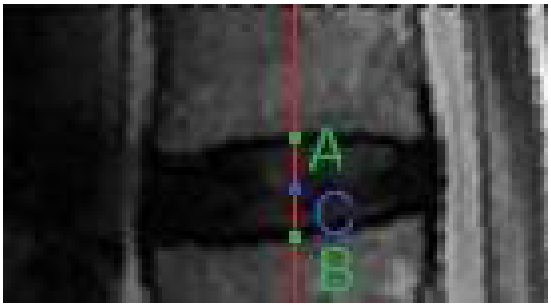


**Fig. 15** The mid-point C between A and B.

## Feature Extraction

### *Selection of ROI from disc for intensity feature extraction*

To obtain a suitable ROI in disc range, feature extraction can be used for in order to classify normal and herniated discs, we act as follows:

At first we considered a cutting in parallel to vertical cutting $X_m$ on disc, and the cross point of the lower and upper edge of disc were called $q$ and $p$, respectively and next, the mid-point between $q$ and $p$ was obtained as that of mid-point C and we called it $r$. Fig. 16 shows this parallel cutting and the mid-point $r$. With points $r$ and $C$, the linear equation, crossing these two points, was obtained and for each of these related images, we achieve to a suitable binary image through extracted discs, as shown in Fig. 16 (right side). The line $d_1$, crossing the points $C$ and $r$, has crossed from the last white pixel at the right side in point $l_1$, and we considered this point as a most straight of disc point. After obtaining the right side point which is actually the right side peak of intensity diagram, we obtained a point in the left side and considered it.

Then by means of four points around the disc we obtain ROI of disc and we draw a rectangle around of disc, as shown in Fig. 17. We can extract intensity feature of discs from this image. The herniated discs have dark pixels in ROI region. One of the main features that Distinguish normal and herniated discs is intensity of discs boundary in T2-waighted of MR images. Thus, the average intensity within the disk drive can be used as a criterion for diagnosis of herniated discs.

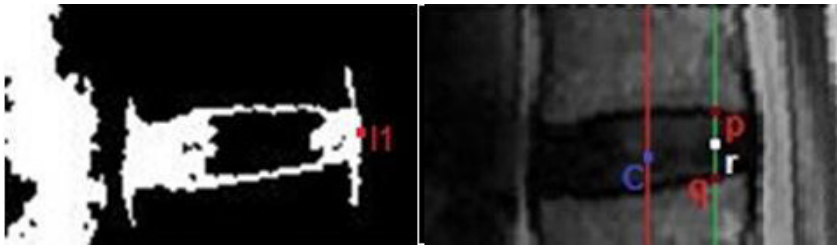


**Fig. 16** Left- binary image of disc by means of Otsu method. Right- two parallel slices inside boundary of disc.

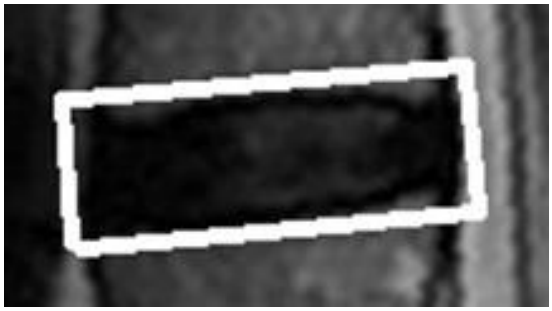

**Fig. 17** Obtained disc ROI by means of four points in top, bottom, left and right.

### *Selection extraction herniated lumbar disc feature*

The most appropriate measure of the radiologists for the diagnosis of lumbar disc herniation is the severely herniated disc. In abnormal disc, substances compress the spinal cord and roots. The degree of lesions depended on nucleus pulpous state. In order for the system to automatically distinguish between normal and herniated disc, in terms of this characteristic, we used the binary images obtained by the Otsu method (Fig. 18).

As shown in Fig. 18, features of a herniated disc is visible at right side of binary Images. Important points that can be used as a suitable measure of binary image of each disc has been shown in Fig. 19 (point "$t$", "$l_1$" and "$b$").

To obtain the coordinates of the point "$t$" in Fig. 18 we started from top right corner of the image, pixel by pixel in the specified range that we saw in Fig. 18, and we store the coordinates of the first pixel with white intensity value as point "$t$". Similarly, the coordinates of the point "b" obtained by storing the first white pixel in the lower right. In the next step, having three points "$t$", "$b$" and "$l_1$", we modeled herniated features with an angle (Fig. 20).

According to the investigation, cases and controls were identified in consultation with the radiologist; there are almost significant differences in abnormal and normal angle of eigenvectors $b\vec{l}_1, t\vec{l}_1$. So get this angle, as a suitable feature for classification.

### *Calculating lengths of the major axis and the minor axis of the disc as shape feature*

We use an important, but simple shape feature $R$ given by $R = a/b \approx$w/h where $a$ and $b$ are the lengths of the major Axis and the minor axis of the disc, respectively: whereas $w$ and $h$ are the width and height of the disc ROI bounding box, respectively (Fig. 21).

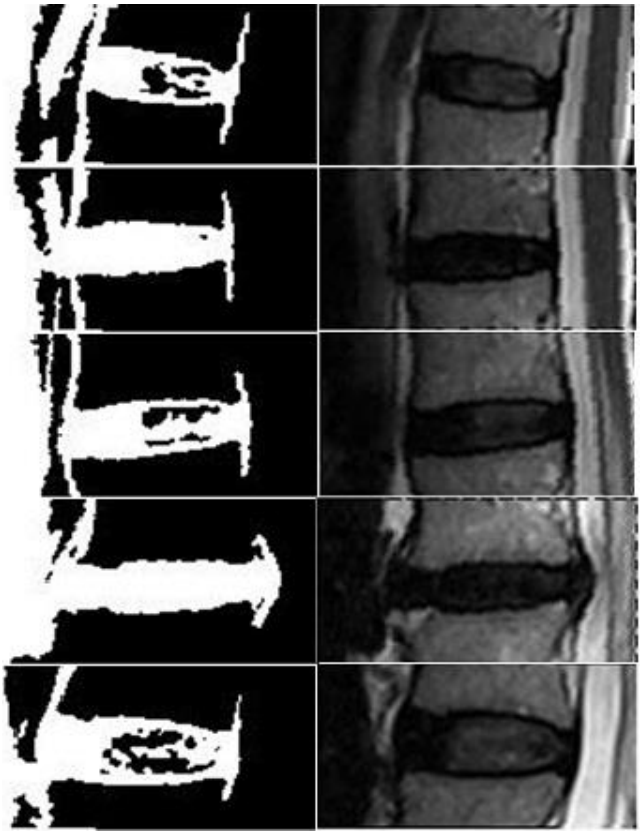

**Fig. 18** Extracted discs from MR images and binarization of them by means of Otsu method for herniation feature extraction.

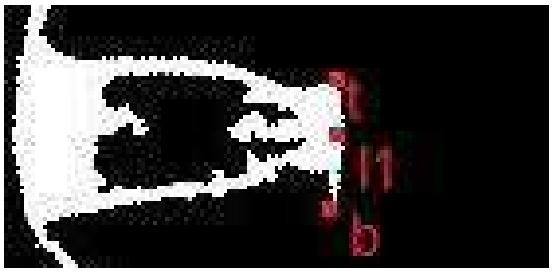


**Fig. 19** The binary image and points "$t$", "$b$" and "$l_1$" on it.


**Fig. 20** Eigenvectors $b\vec{l}_1, t\vec{l}_1$.

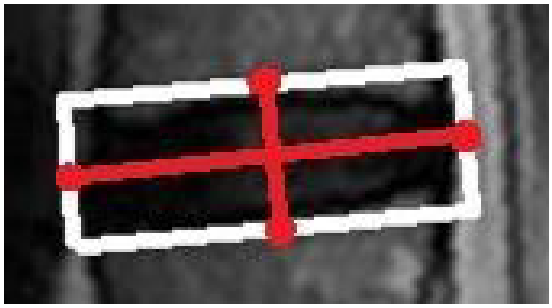

**Fig. 21** Lines of the major axis and the minor axis of the disc.

## EXPERIMENTAL RESULTS

The proposed method in this study has been evaluated through differentiating the patients from normal subjects. The results denote a noticeable capacity in classifying the two classes based on SVM and ANN classifiers. [27–29,23–25,b] In this regard, features are extracted from the disc ROIs, we build two individual classifiers. The first classifier is an SVM, implemented using a linear kernel. This classifier shows 93.80% as accuracy. The second classifier is Artificial Neural Network (ANN) classifier. We train the ANN to classify discs in two classes of normal and herniated. For training the ANN, it has been used 80% of the discs as training set and the rest as test. The ANN classifier shows around 92.38% as accuracy. The statistical measures for validation by SVM and ANN classifiers have been shown in Table 1. The results of our classifiers are shown in Table 2. The performance metrics, the accuracy, sensitivity and specificity are defined as follows:

$$\text{AC} = \frac{\text{TP} + \text{TN}}{\text{TP} + \text{TN} + \text{FN} + \text{FP}}, \tag{18}$$

$$\text{Sensitivity} = \frac{\text{TPs}}{\text{TPs} + \text{FNs}}, \tag{19}$$

**Table 1. The Statistical Measures for Validation by SVM and ANN Classifiers.**

| | TP | FP | FN | TN |
|---|---|---|---|---|
| **SVM** | 37 | 3 | 10 | 160 |
| **ANN** | 35 | 5 | 11 | 159 |

**Table 2. Classifier Performance Results in Percentage for 5-Fold Cross Validation.**

| Classifier | Accuracy | Specificity | Sensitivity |
|---|---|---|---|
| **SVM** | 93.80 | 98.15 | 78.72 |
| **ANN** | 92.38 | 96.95 | 76.08 |

$$\text{Specificity} = \frac{\text{TNs}}{\text{TNs} + \text{FPs}}, \tag{20}$$

where TNs is the Number of True Negatives, FNs is the Number of False Negatives, TPs is the Number of True Positives. FPs is the Number of False Positives.

## DISCUSSION

In this paper, a new approach for diagnosis of disc herniation is proposed. In addition to noticeable classification accuracy, the proposed method is superior to others in terms of its simple implementation. Underpinned by mathematical logics, this method aids to diagnose the disc herniation in a highly accurate, precise and automated manner, eliminating the need to refer to a doctor. Automated diagnostic systems have long been a significant necessity in medical society. Formerly presented methods have failed to fully satisfy this need on account of the corresponding complicated calculations and implementation which lead to less time and cost effectiveness (leading to increased expenses). The suggested method rises above such problems through offering a simpler implementation.

A very important point is the location of disc. In some cases it is just in the midline (Called Central), or near the midline (Para-Central), or lateral, or even far-lateral. In this work, the precise geometrical condition of disks is determined through the proposed mathematical method; it is needless to mention that the extracted information has been a major concern of radiologists.

## CONCLUSION

We proposed a method to detect herniated discs from sagittal and Myelo lumbar MR images using robust intensity and texture features. Initially, we labeled the discs from sagittal images by fitting a third-order polynomial on spinal cord, where we automatically localize a point inside each disc. The major advantage of this method is that, it does not require precise segmentation of the lumbar intervertebral discs. Also, this approach extracts good features which are witnessed from the high accuracies of the SVM and ANN classifiers. Another added advantage is the fact that the final majority voting classifier not only shows a high accuracy and sensitivity; it also elevates the assurance of the diagnosis. As an extension to this approach, we will be

[b]References 25, 28 and 29: Article in Persian with an abstract in English.

working on axial MR images to further decrease the diagnostic error rates. Moreover, we will also work on automatic classification of different subtypes of Herniated Disc which are: bulged, protruded, extruded, fragmented, migrated, and it is very important to define the subtypes.

In other hand, analyzing a more number of features could come in useful when attempting to increase the diagnosis accuracy. Making use of the Mixture of Experts classification, in another sense, ensures a precise decision-making on the output of different areas' processes on the grounds that the final outcome is a product of different decision-makings from various perspectives toward this phenomenon. Through applying what is mentioned above, we pursue improvement of the studies that are conducted in this field.

The segmentation of the normal disc in this approach was very easy but when a disc dehydrates, it is very difficult to find its margins. The mentioned problems continue to exist in our proposed method to spot discs' boundaries, and thus, label the subjects as patients. This could be improved through Image Preprocessing methods in further studies.

## REFERENCES


1. National Institute of Neurological Disorders and Stroke (NINDS), Low back pain fact sheet, NIND Brochure, 2008.
2. Luoma K, Riihimäki H, Luukkonen R, Raininko R, Viikari-Juntura E, Lamminen A, Low back pain in relation to lumbar disc degeneration, *Spine* **25**:487, 2000.
3. Snell RS, Clinical Anatomy by Systems, Lippincott Williams & Wilkins, 2006.
4. Alomari RS, Chaudhary V, Dhillon G, Computer aided diagnosis system for lumbar spine, *4th Int Symp on Appl Sci in Bio Comm Tech (ISABEL)*, Barcelona, Spain, 2011.
5. Rijn JCV, Klemetso N, Reitsma JB, Majoie CBLM, Hulsmans FJ, Peul WC, Stam J, Bossuyt PM, Heeten GJD, Observer variation in MRI evaluation of patients suspected of lumbar disk herniation, *AJR Am J Roentgenol* **184**:299, 2005.
6. Alomari RS, Corso JJ, Chaudhary V, Abnormality detection in lumbar discs from clinical MR images with a probabilistic model, *23rd Int Cong and Exhibition on Comp Assisted Radiol and Surg*, Switzerland, 2009.
7. Alomari RS, Corso JJ, Chaudhary V, Dhillon G, Desiccation diagnosis in lumbar discs from clinical MRI with a probabilistic model, *Proc 6th IEEE Int Conf Symp Biomed Imag: From NanotoMacro (ISBI)*, Boston, MA, pp. 546–549, 2009.
8. Alomari RS, Corso JJ, Chaudhary V, Dhillon G, Computer aided diagnosis of lumbar disc pathology from clinical lower spine MRI, *Int J Comput Assist Radiol Surg* **5**:287, 2010.
9. Michopoulou S, Costaridou L, Panagiotopoulos E, Speller R, Panayiotakis G, Todd-Pokropek A, Atlas-based segmentation of degenerated lumbar intervertebral discs from MR images of the spine, *IEEE Trans Biomedical Imaging* **56**:2225, 2009.
10. Tsai MD, Jou SB, Hsieh MS, A new method for lumbar herniated inter-vertebral disc diagnosis based on image analysis of transverse sections, *Comput Med Imaging Graph (CMIG)* **26**:369, 2002.
11. Jarvik JG, Deyo RA, Diagnostic evaluation of low back pain with emphasis on imaging, *Ann Intern Med* **137**:586, 2002.
12. Graaf I, Prak A, Bierma-Zeinstra S, Thomas S, Peul W, Koes B, Diagnosis of lumbar spinal stenosis: A systematic review of the accuracy of diagnostic tests, *Spine* **31**:1168, 2006.
13. Bounds DG, Lloyd PJ, Mathew B, Waddell G, A multilayer perceptron network for the diagnosis of low back pain, *IEEE Int Conf on Neur Net IEEE Cat*, No. 88CH2632-8, pp. 481–489, 1988.
14. Wildermuth S, Zanetti M, Duewell S, Schmid MR, Romanowski B, Benini A, Boni T, Hodler J, Lumbar spine: Quantitative and qualitative assessment of positional (upright flexion and extension) MR imaging and myelography, *Radiology* **207**:391, 1998.
15. Vaughn, M, Using an artificial neural network to assist orthopaedic surgeons in the diagnosis of low back pain, http://www.marilyn-vaughn.co.uk/lbpainresearchstudy.htm, Dept. of Inf., Cranfield University (RMCS), June 2000.
16. Roberts N, Gratin C, Whitehouse GH, MRI analysis of lumbar intervertebral disc height in young and older populations, *J Magn Reson Imaging* **7**:880, 1997.
17. Roberts M, Cootes T, Pacheco E, Adams J, Quant. vertebral fracture detection on dxa images using shape and appearance models, *Acad Radiol* **14**:1166, 2007.
18. Chevrefils C, Chériet F, Grimard G, Aubin C, Watershed segmentation of intervertebral disk and spinal canal from MRI images, *Lecture Notes in Comput Sci ICIAR*, pp. 1017–1027, 2007.
19. Alomari RS, Corso JJ, Chaudhary V, Dhillon G, Toward a clinical lumbar cad: Herniation diagnosis, *Int J Comput Assist Radiol Surg* **6**:119, 2011.
20. Liao PS, Chen TS, Chung PC, A fast algorithm for multilevel thresholding, *J Inform Sci Eng* **17**:713, 2001.
21. Senthilkumaran N, Vaithegi S, Image segmentation by using thresholding techniques for medical images, *Comput Sci Eng Int J (CSEIJ)* **6**:1, 2016
22. Athertya J, Kumar G, Fuzzy clustering based segmentation of vertebrae in T-1 Weighted spinal MR images, *Int J Fuzzy Logic Sym (IJFLS)* **6**:2, 2016
23. Ebrahimzadeh E, Pooyan M, Bijar A, A novel approach to predict sudden cardiac death (SCD) using nonlinear and time-frequency analyses from HRV signals, *PLoS ONE* **9**:1, 2014.
24. Ebrahimzadeh E, Pooyan M, Early detection of sudden cardiac death by using classical linear techniques and time-frequency methods on electrocardiogram signals, *Biomed Sci Eng* **11**:699, 2011.

25. Ebrahimzadeh E, Pooyan M, Prediction of sudden cardiac death (SCD) using time-frequency analysis of ECG signals, *Int Soc Environ Epidemiol* **3**:15, 2013.
26. Ebrahimzadeh E, Pooyan M, Jahani S, Bijar A, Setaredan SK, ECG Signals noise removal: Selection and optimization of the best adaptive filtering algorithm based on various algorithms comparison, *Biomed Eng Appl Basis Commun* **27**:1550038, 2015.
27. Ebrahimzadeh E, Alavi SM, Bijar A, Pakkhesal AR, A novel approach for detection of deception using smoothed pseudo Wigner-Ville distribution (SPWVD), *J Biomed Sci Eng* **6**:8, 2013.
28. Ebrahimzadeh E, Alavi SM, Samsami Khodadad F, Implementation and designing of lie-detection system based on electroencephalography (EEG), *Sci Res J Army Univ Med Sci I.R. Iran* **11**:20, 2013.
29. Amoozegar S, Pooyan M, Ebrahimzadeh E, Classification of brain signals in normal subjects and patients with epilepsy using mixture of experts, *Int Soc Environ Epidemiol* **4**:1, 2013.